

**DYNAMIC JAHN-TELLER EFFECT AND SUPERCONDUCTING
EXCITATIONS IN RAMAN SPECTRA**

B. K. RAJ

*Department of Physics, Government (Autonomous) College,
Angul-759128, India*

B. PRADHAN*

*Department of Physics, Government Science College,
Malkangiri-764048, India*

G. C. ROUT†

*Department of Physics, School of Applied Sciences,
KIIT, University, Bhubaneswar-751024, India.*

We report a model study of the phonon response on the interplay of the superconducting (SC) gap and both static and dynamic Jahn-Teller distortion and predict the appearance of the SC and Jahn-Teller (JT) distortion gap excitation peaks in the Raman spectra of high- T_c superconductors. The model consists of the Hamiltonian containing static JT interaction and s -wave type SC interaction in the conduction band. Further the phonons are coupled to the density of the conduction electron in the band as well as to the JT split conduction band giving rise to dynamic Jahn-Teller (DJT) interaction. The phonons are considered in a harmonic approximation. The phonon Green's function is calculated by Zubarev's technique and the phonon self-energy arising due to normal electron-phonon (EP) interaction and DJT interaction. The phonon self-energy arising due to this is calculated from the electron response density function in the coexistence phase of the two order parameters. The phonon spectral density predicts two excitation peaks, one due to SC gap and the other due to JT distortion. The DJT coupling suppresses the JT gap while it enhances SC gap as well as SC transition temperature. The evolution of these excitation peaks are investigated by varying different model parameters of the system.

Keywords: High- T_c Superconductivity; Dynamic Jahn-Teller Effect; Electron-Phonon Interaction; Raman spectra.

1. Introduction

The structural transition plays dominant role on various physical properties as well as on the occurrence of superconductivity in some of the high- T_c cuprates. The

*Corresponding author, Email: brunda@iopb.res.in, Mob: +91-9437806565

†Email: gcr@iopb.res.in: Mobile: +91-9937981694

system $La_{1-x}Ba_xCuO_4$ (LBCO) with $x = 0.15$ shows a phase transition from high temperature tetragonal to low temperature orthorhombic phase at $T_d = 180K$ accompanied by the SC phase transition at $35K$ at the onset of superconductivity. The neutron diffraction on LBCO shows an orthorhombic phase below $T = 180K$ ^{1,2,3}. The orthorhombic structure of the system $La_{2-x}Sr_xCuO_4$ (LSCO) changes near the SC transition temperature $T_c \simeq 36K$, but a structural transition takes place at $T_d = 220K$ ⁴. The thermal expansion measurements on the cuprate systems of Lang *et al*³ demonstrates that the high- T_c is observed at optimum doping for which the system undergoes the tetragonal to orthorhombic transition. The structural transition associated with the lowering of the crystallographic symmetry has also been observed in other high- T_c cuprates^{5,6,7}. Besides the system LSCO the other high- T_c superconductors (HTSCs) also exhibit similar anomalies in the isotope effect exponent. A correlation between the superconducting transition temperature and the scattering intensity from $43cm^{-1}$ and $100cm^{-1}$ modes for bismuthates are studied by Sugai *et al*⁸.

The experimental data shows that the isotope shift exponent (α) of HTSCs shows the influence of structural phase transition. It is observed that the transition temperature T_c is enhanced with the increase of dopant concentration, while α decreases monotonically. The experiments on LSCO by Crawford *et al*^{9,10} gives the higher value of α than the BCS value of $\alpha = 0.5$ calculated from the phonon mechanism of pairing. It is generally noticed that value of isotope exponent α is smaller than 0.5. The LSCO system gives a highest SC transition temperature of $T_c^{max} = 38K$ at optimum doping. Further, it is observed that the T_c decreases with the decrease of dopant concentration while the value of α increases from 0.1 to 0.6. These variations can be understood if the system undergoes a structural phase transition.

The band Jahn-Teller (BJT) distortion usually induces structural phase transition. The lattice strain removes the degeneracy in the conduction electron states by lowering the lattice symmetry. The system is stabilized due to the gain in electronic energy at the cost in the elastic energy. In the strained state, the conduction band is maximally occupied. For large distortion, the gap due to BJT distortion produces an insulating phase. In this scenario the doping of the holes modifies the occupation probabilities of the two bands.

For the first time Raman scattering exhibit SC gap excitation mode in the layered system $2H-NbSe_2$ ^{11,12}, where Raman peak has coupled to the charge density wave (CDW) amplitude mode of the system. They have observed SC gap excitation mode at $16cm^{-1}$ and CDW amplitude mode at $40cm^{-1}$ in the Raman spectra due to the coupling of SC gap to the CDW amplitude phonon. Several authors^{13,14,15,16} have tried to explain the origin of the collective modes of the SC and CDW state appearing in Raman spectra. Recently Rout *et al*¹⁷ have reported the interplay of JT distortion and superconductivity into Raman active excitation peaks. It is to note that the authors have considered only static JT distortion in their calculation.

More recently Raj *et al*¹⁸ have considered the interplay of superconductivity and static JT distortion in presence of a DJT distortion and reported the results for modified BCS type gap equation which is strongly influenced by DJT distortion. Based on the same model¹⁸ we calculate here phonon Green's function and report Raman active excitation peaks which can explain the Raman scattering observed in high- T_c cuprates, layered 2H-NbSe₂^{11,12} as well as the high- T_c system like bismuthates [$K_xBa_{1-x}BiO_3$]⁸. The rest of the work is organized as the theoretical model in section 2, the phonon self-energy is calculated in section 3, the electron response function in section 4, Raman spectral intensity is presented in section 5, the results are discussed in section 6 and finally concluded in section 7.

2. Theoretical Model

The present model study attempts to investigate the effect of dynamic Jahn-Teller distortion on the superconducting gap in high- T_c superconductors. In order to introduce JT effect in the conduction band we consider two orbitals ($\alpha = 1, 2$) which was splitted due to the introduction of the JT effect. In order to represent SC, static JT and DJT effect we write the Hamiltonian below based upon our earlier models^{18,17,19,20}.

$$H_c = \sum_{k\sigma} \epsilon_k \left(c_{1k\sigma}^\dagger c_{1k\sigma} + c_{2k\sigma}^\dagger c_{2k\sigma} \right) \quad (1)$$

$$H_{e-L} = Ge \sum_{k\sigma} \left(c_{1k\sigma}^\dagger c_{1k\sigma} - c_{2k\sigma}^\dagger c_{2k\sigma} \right) \quad (2)$$

The Hamiltonian H_c represents the hopping of the electrons between the two nearest neighbors for the two degenerate orbitals designated as 1 and 2. The dispersion of the degenerate band in a two dimensional CuO₂ plane is written as $\epsilon_k = -2t_0(\cos k_x + \cos k_y)$. Here $c_{\alpha k\sigma}^\dagger$ ($c_{\alpha k\sigma}$), for $\alpha = 1$ and 2, are creation (annihilation) operators of the conduction electrons of copper ions for two orbitals with momentum k and spin σ . The Hamiltonian H_{e-L} represents the static JT interaction where G is the strength of the electron-lattice interaction and e is the strength of the isotropic static lattice strain. The lattice strain splits the single degenerate band into two bands with energies $\epsilon_{1k,2k} = \epsilon_k \pm Ge$. The elastic energy of the system is $\frac{1}{2}Ce^2$ with C representing the elastic constant. The minimization of the free energy of the electron including the elastic energy helps to find the expression for lattice strain. It is shown earlier^{17,19,20} that the static lattice strain suppresses the SC gap parameter in the interplay region of the two order parameters.

In order to investigate the phonon response in the HTSCs, we consider the phonon interaction to the density of the conduction electrons of both the orbitals as well as the phonon coupling to the difference in electron densities of the JT distorted orbitals of the conduction band. The electron-phonon interaction Hamiltonian is

written as

$$\begin{aligned} H_{e-p} &= \sum_{\alpha,k,\sigma} f_1(q) \left(c_{\alpha,k+q,\sigma}^\dagger c_{\alpha,k,\sigma} \right) A_q - \sum_{\alpha,k,\sigma} (-1)^\alpha f_2(q) e \left(c_{\alpha,k+q,\sigma}^\dagger c_{\alpha,k,\sigma} \right) A_q \\ &= \sum_{\alpha,k,\sigma} s_\alpha(q) \left(c_{\alpha,k+q,\sigma}^\dagger c_{\alpha,k,\sigma} \right) A_q. \end{aligned} \quad (3)$$

The strength of the electron-phonon coupling $s_\alpha(q)$ is defined as $s_\alpha = f_1(q) - (-1)^\alpha f_2(q)e$ in which $f_1(q)$ is the normal EP coupling and $f_2(q)$ is the dynamic Jahn-Teller EP coupling. The q^{th} -Fourier component of the phonon displacement operator is $A_q = b_q + b_{-q}^\dagger$ with b_q^\dagger (b_q) defining the phonon creation (annihilation) operator for wave vector q . Further the free phonon Hamiltonian H_p is given in harmonic approximation as

$$H_p = \sum_q \omega_q b_q^\dagger b_q, \quad (4)$$

with ω_q being the free phonon frequency.

Our main objective in the present report is to study the effect of dynamic JT distortion on the superconductivity in HTSCs. The d -wave models have gained substantial support recently over s -wave pairing as the mechanism by which high temperature superconductivity might be explained. The establishment of d -wave symmetry in cuprates does not necessarily specify a high- T_c mechanism. It does not impose well defined constraints on possible models for this mechanism. While the spin fluctuation pairing mechanism leads naturally to an ordered parameter with d -wave symmetry, the conventional BCS electron phonon pairing interaction give rise to s -wave superconductivity. Müller^{21,22} has considered d -wave symmetry near the surface and s -wave symmetry in bulk of cuprate superconductors and applied them to small angle neutron scattering results. Zhao²³ has concluded from angle-resolved photo-emission spectroscopy and scanning tunneling spectroscopy that the superconductivity is extended s -wave rather than d -wave. So it is not definite that the bulk superconductivity is d -wave. We consider here the s -wave pairing interaction within the same orbitals and the same strength of interactions for the two orbitals. The BCS type pairing Hamiltonian is considered here for the two orbitals as

$$H_I = -\Delta \sum_{\alpha,k} \left(c_{\alpha,k,\uparrow}^\dagger c_{\alpha,-k,\downarrow}^\dagger + c_{\alpha,-k,\downarrow} c_{\alpha,k,\uparrow} \right). \quad (5)$$

In order to simulate an attractive interaction to produce Cooper pairs, the energy dependence of the interaction potential is taken as

$$U(\epsilon) = U_0 \left[1 - \frac{(\epsilon - \epsilon_F)^4}{\omega_D^4} \right]^{\frac{1}{2}}, \quad (6)$$

where U_0 is the effective attractive Coulomb interaction, ω_D is cut-off energy and ϵ_F represents the Fermi energy. In order to produce band splitting due to JT distortion, we consider an energy dependent density of state $N(\epsilon)$ around the center of the

conduction band in the system. Such a logarithmic model density of state²⁰ is given by

$$N(\epsilon) = N(0) \sqrt{1 - \left| \frac{\epsilon}{D} \ln \left| \frac{D^2}{\epsilon^2} \right| \right|}, \quad (7)$$

where $2D = W$ is the conduction band width. The total Hamiltonian describing the DJT effect and SC interaction in high- T_c cuprate systems can be written as

$$H = H_c + H_{e-L} + H_I + H_{e-p} + H_p. \quad (8)$$

The phonon induced superconductivity given in eqn.(5) is the consequence of the electron-phonon interaction. Here we have included the phonon mediated superconducting pairing as well as the normal electron-phonon interaction and both the static and dynamic band Jahn-Teller interactions in the total Hamiltonian in order to study their effect on the superconducting gap. The appearance of the Debye frequency ω_D in the energy dependence of repulsive Coulomb energy in eqn.(6) implies that the pairing interaction is mediated via phonons. The electron-phonon interaction which is considered explicitly in eqn.(3) is just a very small interaction contributing negligibly to the pairing. However, the main interest in the present work is to investigate the effect of Jahn-Teller strain on the pairing and the superconducting gap as well.

3. Phonon self-energy for finite q

The phonon self-energy for the system is evaluated by the double-time Green's function technique of Zubarev²⁴ using the equation of motion method. The single particle phonon Green's function is defined as

$$\begin{aligned} D_{qq'}(t - t') &= \langle \langle A_q(t); A_{q'}(t') \rangle \rangle \\ &\equiv -i\theta(t - t') \langle [A_q(t); A_{q'}(t')] \rangle. \end{aligned} \quad (9)$$

Using the total Hamiltonian of eqn.(8), the Fourier transformed phonon Green's function reduces to

$$D_{qq'}(\omega) = \delta_{-qq'} D_q^0(\omega) + 2\pi s_\alpha^2 D_q^0(\omega) \chi_{qq'}(\omega) D_{q'}^0(\omega), \quad (10)$$

where the Fourier transformed free phonon propagator is given by

$$D_q^0(\omega) = \frac{\omega_q}{\pi(\omega^2 - \omega_q^2)}. \quad (11)$$

Applying Dyson's approximation, the eqn.(10) can be written in a closed form as

$$D_{qq'}(\omega) = \frac{1}{\pi} \frac{\omega_q}{[\omega^2 - \omega_q^2 - \sum(\omega, q)]}, \quad (12)$$

where the phonon self-energy appears as

$$\sum(\omega, q) = 4\pi\omega_q \chi_{qq'}(\omega), \quad (13)$$

$\chi_{qq'}(\omega)$ is the electron density response function, which consists of the contributions from the two degenerate orbitals 1 and 2 as $\chi_{qq'}(\omega) = \chi_{qq'}^1(\omega) + \chi_{qq'}^2(\omega)$ and the electron-phonon coupling parameters $s_\alpha = f_1 \pm f_2 \times e$. The two response functions corresponding to the two orbitals are given by

$$\chi_{qq'}^1(\omega) = \sum_{k\sigma k'\sigma'} s_\alpha^2 \Gamma_1(k, \sigma, k', \sigma', q, q', \omega), \quad (14)$$

$$\chi_{qq'}^2(\omega) = \sum_{k\sigma k'\sigma'} s_\alpha^2 \Gamma_2(k, \sigma, k', \sigma', q, q', \omega), \quad (15)$$

with

$$\Gamma_1(k, q, \sigma, \omega) = \Gamma_1^a(k, -q, \omega) + \Gamma_1^b(k, -q, \omega), \quad (16)$$

$$\Gamma_2(k, q, \sigma, \omega) = \Gamma_2^a(k, -q, \omega) + \Gamma_2^b(k, -q, \omega). \quad (17)$$

Further the two particle Green's functions Γ_1 and Γ_2 contain the other Green's functions defined as

$$\Gamma_1^a(k, -q, \omega) = \langle \langle \alpha_k^a; \chi_{1k'} \rangle \rangle_\omega, \Gamma_1^b(k, -q, \omega) = \langle \langle \alpha_k^b; \chi_{1k'} \rangle \rangle_\omega, \quad (18)$$

$$\Gamma_2^a(k, -q, \omega) = \langle \langle \alpha_k^a; \chi_{2k'} \rangle \rangle_\omega, \Gamma_2^b(k, -q, \omega) = \langle \langle \alpha_k^b; \chi_{2k'} \rangle \rangle_\omega. \quad (19)$$

The new two particle Green's functions are expressed in terms of the electron density operators like α_k^a , α_k^b , β_k^b , β_k^b , $X_{1k'}$, $X_{2k'}$, which are defined below:

$$\begin{aligned} \alpha_k^a &= C_{1k-q\uparrow}^\dagger C_{1k\uparrow}, \alpha_k^b = C_{1k-q\downarrow}^\dagger C_{1k\downarrow}, \\ \beta_k^a &= C_{2k-q\uparrow}^\dagger C_{2k\uparrow}, \beta_k^b = C_{2k-q\downarrow}^\dagger C_{2k\downarrow}, \\ \chi_{1k'} &= C_{1k'-q',\sigma'}^\dagger C_{1k'\sigma'}, \chi_{2k'} = C_{2k'-q',\sigma'}^\dagger C_{2k'\sigma'}. \end{aligned} \quad (20)$$

4. Electron response function for finite q

For the calculation of the two particle Green's function $\Gamma_1(k - q, \omega)$ for the JT split orbital 1, the other higher order Green's functions involving superconducting and normal state operators are defined as

$$\begin{aligned} A_1^a(k, \omega) &= \langle \langle \gamma_k^1; X_{1k'} \rangle \rangle_\omega, \quad A_1^b(k, \omega) = \langle \langle \gamma_k^2; X_{1k'} \rangle \rangle_\omega, \\ A_2^a(-k + q, \omega) &= \langle \langle \gamma_{-k+q}^1; X_{1k'} \rangle \rangle_\omega, \quad A_2^b(-k + q, \omega) = \langle \langle \gamma_{-k+q}^2; X_{1k'} \rangle \rangle_\omega, \\ A_3^a(-k + q, \omega) &= \langle \langle \alpha_{-k+q}^a; X_{1k'} \rangle \rangle_\omega, \quad A_3^b(-k + q, \omega) = \langle \langle \alpha_{-k+q}^b; X_{1k'} \rangle \rangle_\omega. \end{aligned}$$

The SC Green's functions A_1 , A_2 , A_3 involve the two particle Cooper pairing operators as defined below

$$\begin{aligned} \gamma_k^1 &= C_{1,k-q\uparrow}^\dagger C_{1,-k\downarrow}^\dagger, \quad \gamma_k^2 = C_{1,-k+q\downarrow} C_{1,k\uparrow}, \\ \gamma_{-k+q}^1 &= C_{1,-k\uparrow}^\dagger C_{1,k-q\downarrow}^\dagger, \quad \gamma_{-k+q}^2 = C_{1,k\downarrow} C_{1,-k+q\uparrow}. \end{aligned} \quad (21)$$

The new Green's functions are related to each other as

$$\begin{aligned} A_1(k, \omega) &= A_1^a(k, \omega) - A_1^b(k, \omega), \\ A_2(-k + q, \omega) &= A_2^a(-k + q, \omega) - A_2^b(-k + q, \omega), \\ A_3(-k + q, \omega) &= A_3^a(-k + q, \omega) - A_3^b(-k + q, \omega). \end{aligned} \quad (22)$$

Similarly for the calculation of the two particle Green's function $\Gamma_2(k - q, \omega)$ corresponding to the orbital 2, the other higher order Green's functions involving superconducting and normal state operators are defined as

$$B_1^a(k, \omega) = \langle \langle \delta_k^1; X_{2k'} \rangle \rangle_\omega, \quad B_1^b(k, \omega) = \langle \langle \delta_k^2; X_{2k'} \rangle \rangle_\omega, \quad (23)$$

$$B_2^a(-k + q, \omega) = \langle \langle \delta_{-k+q}^1; X_{2k'} \rangle \rangle_\omega, \quad B_2^b(-k + q, \omega) = \langle \langle \delta_{-k+q}^2; X_{2k'} \rangle \rangle_\omega, \quad (24)$$

$$B_3^a(-k + q, \omega) = \langle \langle \alpha_{-k+q}^a; X_{2k'} \rangle \rangle_\omega, \quad B_3^b(-k + q, \omega) = \langle \langle \alpha_{-k+q}^b; X_{2k'} \rangle \rangle_\omega. \quad (25)$$

The SC Green's functions B_1 , B_2 , B_3 involve the two particle Cooper pairing operators as defined below

$$\begin{aligned} \delta_k^1 &= C_{2,k-q\uparrow}^\dagger C_{2,-k\downarrow}^\dagger, \quad \delta_k^2 = C_{2,-k+q\downarrow} C_{2,k\uparrow}, \\ \delta_{-k+q}^1 &= C_{2,-k\uparrow}^\dagger C_{2,k-q\downarrow}^\dagger, \quad \delta_{-k+q}^2 = C_{2,k\downarrow} C_{2,-k+q\uparrow}. \end{aligned} \quad (26)$$

The new Green's functions defined in equations(23)-(25), are again related as

$$\begin{aligned} B_1(k, \omega) &= B_1^a(k, \omega) - B_1^b(k, \omega), \\ B_2(-k + q, \omega) &= B_2^a(-k + q, \omega) - B_2^b(-k + q, \omega), \\ B_3(-k + q, \omega) &= B_3^a(-k + q, \omega) - B_3^b(-k + q, \omega). \end{aligned} \quad (27)$$

The electron response functions $\chi_{qq'}^1(\omega)$ and $\chi_{qq'}^2(\omega)$ are calculated for the two orbitals separately and the two are added together to get the final result. The frequency (ω) and wave vector (q) dependent total electron response function at finite temperature then can be written as

$$\begin{aligned} \chi_{qq}(\omega) &= \chi_{qq}^1(\omega) + \chi_{qq}^2(\omega) \\ &= \frac{1}{2\pi} \sum_{k\alpha} \frac{1}{|D_\alpha|} [(\omega^2 - \epsilon_{\alpha+}^2(k, q))(\omega - \epsilon_{\alpha-}(k, q)) \\ &\quad \times (n_{\alpha,k-q} - n_{\alpha,k}) + 4\omega\Delta(\omega - \epsilon_{\alpha-}(k, q))(\phi_{\alpha,k-q} + \phi_{\alpha,k})], \end{aligned} \quad (28)$$

where $\alpha = 1$ and 2 , $n_{\alpha,k-q} = n_{\alpha,k-q\uparrow} + n_{\alpha,k-q\downarrow}$ and the denominator

$$|D_\alpha| = (\omega^2 - \tilde{E}_{\alpha+}^2(k, q))(\omega^2 - \tilde{E}_{\alpha-}^2(k, q)) \quad (29)$$

with $\tilde{E}_{\alpha,\pm}(k, q) = \tilde{E}_{\alpha,k-q} \pm \tilde{E}_{\alpha,k}$, $\epsilon_{\alpha\pm}(k, q) = \epsilon_{\alpha,k-q} \pm \epsilon_{\alpha,k}$ and $\tilde{E}_{\alpha,k}^2 = (\tilde{\epsilon}_{\alpha,k}^2 + \tilde{\Delta}_\alpha^2)$ are the energy of the SC gap excitation, with $\epsilon_{1k-q} = (\epsilon_{k-q} + Ge)$ and $\epsilon_{2k-q} = (\epsilon_{k-q} - Ge)$. In presence of normal EP coupling and the DJT coupling, the renormalized conduction band dispersion $\tilde{\epsilon}_{\alpha,k}$ and the SC gap $\tilde{\Delta}_\alpha$ are given in equations(32) and (33) respectively. The SC amplitudes $\phi_{\alpha,k}$ are given by

$$\phi_{\alpha,k} = \langle C_{\alpha,k\uparrow}^\dagger C_{\alpha,-k\downarrow}^\dagger \rangle = \frac{\tilde{\Delta}_\alpha}{2\tilde{E}_{\alpha,k}} \tanh\left(\frac{\beta\tilde{E}_{\alpha,k}}{2}\right). \quad (30)$$

The SC gap (Δ) and the lattice strain due to JT distortion (e) are temperature dependent quantities which can be determined self-consistently.

In order to calculate the Raman spectrum, it is necessary to evaluate the electron response function in the limit $q \rightarrow 0$, at a finite temperature ($T \neq 0$). The electron response function in the limit $q = 0$ reduces to

$$\chi(\omega, q = 0) = \frac{1}{2\pi} \sum_{\alpha, k} \left[\frac{8\tilde{\Delta}_\alpha \phi_{\alpha, k}}{\omega^2 - 4\tilde{E}_{\alpha, k}^2} \right], \quad (31)$$

where $\tilde{E}_{\alpha, k}^2 = \tilde{\epsilon}_{\alpha, k}^2 + \tilde{\Delta}_\alpha^2$ with

$$\tilde{\epsilon}_{\alpha k} = \epsilon_{\alpha k} + s_\alpha^2 \left[\frac{(\omega - \epsilon_{\alpha k})N_0}{(\omega - \epsilon_{\alpha k})^2 + \Delta^2} \right], \quad (32)$$

and

$$\tilde{\Delta}_{\alpha k} = \Delta + s_\alpha^2 \left[\frac{\Delta N_0}{(\omega - \epsilon_{\alpha k})^2 + \Delta^2} \right] \quad (33)$$

where

$$N_0 = 2(e^{\beta\omega_0} - 1)^{-1},$$

with $\beta = 1/k_B T$ and ω_0 being the bare phonon frequency at temperature T.

$$\chi(\omega + i\eta, q = 0) = \frac{1}{2\pi} \sum_{\alpha, k} 8\tilde{\Delta}_\alpha \phi_{\alpha, k} \left[\frac{\omega^2 - 4\tilde{E}_{\alpha, k}^2}{|D_{\alpha 0}|} - i \frac{2\eta\omega}{|D_{\alpha 0}|} \right] \quad (34)$$

$$\sum (\omega + i\eta, q = 0) = 16\omega_0 \sum_{\alpha, k} \tilde{\Delta}_\alpha s_\alpha^2 \phi_{\alpha, k} \left[\frac{\omega^2 - 4\tilde{E}_{\alpha, k}^2}{|D_{\alpha 0}|} - i \frac{2\eta\omega}{|D_{\alpha 0}|} \right] \quad (35)$$

where $|D_{\alpha 0}| = (\omega^2 - 4\tilde{E}_{\alpha, k}^2)^2 + 4\eta^2\omega^2$.

The temperature dependent SC gap (Δ) and lattice strain (e) are calculated by using the total Hamiltonian given in equations(1) to (4). The calculations within a mean-field approximation give rise to a modified BCS type gap equation with involving renormalized conduction band dispersion $\tilde{\epsilon}_{\alpha k}$ and the renormalized SC gap parameter $\tilde{\Delta}_\alpha$ has written in equations(32) and (33). The SC gap equation and the lattice strain are calculated in terms of these renormalized quantities and the equations are

$$1 = \int_{-\omega_D}^{\omega_D} U(\epsilon) N(\epsilon) d\epsilon_k \left[\frac{1}{2\tilde{E}_{1k}} \tanh \left(\frac{1}{2} \beta \tilde{E}_{1k} \right) + \frac{1}{2\tilde{E}_{2k}} \tanh \left(\frac{1}{2} \beta \tilde{E}_{2k} \right) \right], \quad (36)$$

$$e = \left(\frac{-G}{C_0} \right) \int_{-W/2}^{W/2} N(\epsilon) d\epsilon_k \left[\frac{\tilde{\epsilon}_{1k}}{2\tilde{E}_{1k}} \tanh \left(\frac{1}{2} \beta \tilde{E}_{1k} \right) - \frac{\tilde{\epsilon}_{2k}}{2\tilde{E}_{2k}} \tanh \left(\frac{1}{2} \beta \tilde{E}_{2k} \right) \right]. \quad (37)$$

These two gap equations are solved numerically and self-consistently and reported earlier¹⁸. The values of SC gap Δ and lattice strain e are calculated on the numerical solution at a particular temperature and later on used for the calculation of Raman spectra at a given finite temperature.

5. Raman spectra in the limit $q = 0$ at finite T

The Raman intensity is given by the spectral density function (SDF) of the zone center phonon. The SDF in general is defined by

$$S(\omega, q) = -\pi \text{Im} D_{qq'}(\omega)|_{\eta \rightarrow 0} \quad (38)$$

where the phonon Green's function $D_{qq'}(\omega)$ is given in equation(12). At the limit $q = 0$ and finite temperature (T) we have

$$D_{00}(\omega + i\eta) = \frac{1}{\pi} \left[\frac{\omega_0(A_1 - iB_1)}{A_1^2 + B_1^2} \right], \quad (39)$$

and hence

$$S(\omega, q = 0) = \frac{\omega_0 B_1}{A_1^2 + B_1^2} \quad (40)$$

where A_1 and B_1 are

$$A_1 = \omega^2 - \omega_0^2 - A_2, \quad B_1 = 2\eta\omega - B_2, \quad (41)$$

with $A_2 = 8\omega_0 \sum_{\alpha} s_{\alpha}^2 \int N(0) r d\epsilon_k G_{\alpha}$ and $B_2 = -16\omega_0 \eta \sum_{\alpha} s_{\alpha}^2 \int N(0) r d\epsilon_k H_{\alpha}$ where

$$G_{\alpha} = \left[\frac{\tilde{\Delta}_{\alpha}^2(\omega^2 - 4\tilde{E}_{\alpha k}^2)}{\tilde{E}_{\alpha k} |D_{\alpha 0}|} \tanh \left(\frac{\beta \tilde{E}_{\alpha k}}{2} \right) \right], \quad (42)$$

$$H_{\alpha} = \left[\frac{\tilde{\Delta}_{\alpha}^2}{\tilde{E}_{\alpha k} |D_{\alpha 0}|(\omega)} \tanh \left(\frac{\beta \tilde{E}_{\alpha k}}{2} \right) \right]. \quad (43)$$

The different physical quantities of the atomic subsystem are made dimensionless dividing them by the hopping integral $2t_0$, the width of the conduction band is $W = 8t_0$. The dimensionless parameters are the SC gap parameter $z = \frac{\Delta}{2t_0}$, the SC coupling parameter $g = N(0)U_0$, the Debye frequency $\omega_D = \frac{\omega_D}{2t_0}$, the reduced temperature $t = \frac{k_B T}{2t_0}$, the reduced incident photon frequency $c_1 = \frac{\omega}{2t_0}$, the phonon vibrational frequency $\omega_1 = \frac{\omega_q}{2t_0}$, the reduced bare phonon frequency $p = \frac{\omega_0}{2t_0}$, $x = \frac{\epsilon_k}{2t_0}$, $e_q = \frac{qv_f}{2t_0}$, the JT coupling constant $g_1 = \frac{G}{2t_0}$, the reduced lattice strain $\tilde{e} = \frac{e}{2t_0}$, the normal electron-phonon coupling $\lambda_1 = \frac{f_1}{2t_0}$, the dynamic electron-phonon coupling $\lambda_2 = \frac{f_2}{2t_0}$, spectral width $e_1 = \frac{\eta}{2t_0}$ and we have taken the JT distortion energy $e' = g_1 \times \tilde{e}$.

6. Results and Discussion

Before calculating the spectral density function (SDF) under dynamic condition of JT effect at a finite temperature, we solved the SC gap parameter (z) and lattice strain (e'). The self-consistent solution of these two temperature dependent parameters are plotted in figure 1. Earlier the solution for z and e' are solved self-consistently under static and dynamic limits of JT effect and the results are reported¹⁸. It has been observed that the lattice strain is suppressed throughout

the temperature range under the DJT condition and the SC gap (z) is enhanced accompanied by an enhancement in transition temperature t_c . However, the temperature dependencies of these two parameters in static limit are similar to their counter part in the dynamic limit. It is concluded from this that at a given temperature the SC gap in dynamic limit is larger than its value in static limit, whereas the magnitude of the lattice strain has lesser value in dynamic limit than in static limit. Accordingly the Raman excitation peaks in dynamic limit is expected to appear at slightly displaced position than that of the static limit. The evolution of these Raman peaks will be studied in the present investigation by varying the model electronic as well as lattice parameters of the system as shown in subsequent figures from 2 to 9. In the present case figure 1 shows the temperature dependent SC gap (z) and lattice strain (e') under dynamic limit of the DJT effect. In this case the SC transition temperature appears at $t_c \simeq 0.0052$ and the lattice distortion temperature appears at $t_d \simeq 0.0082$. It is to note further that lattice strain is suppressed at lower temperatures where the superconductivity coexists with lattice distortion.

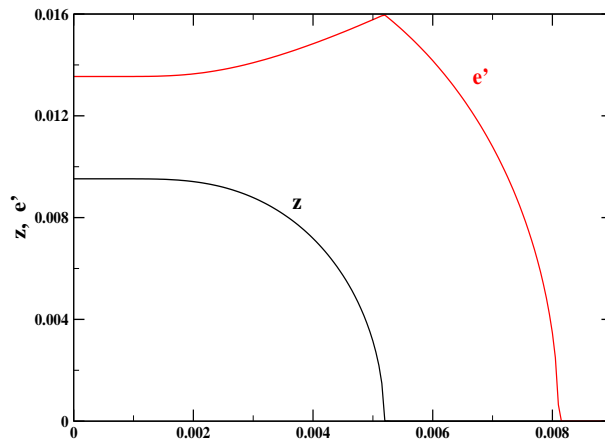


Fig. 1 The self-consistent plots of SC gap z and JT gap energy e' vs. reduced temperature t for the SC coupling $g = 0.031$, the static JT coupling $g_1 = 0.152$, the phonon vibrational frequency $\omega_1 = 0.06$, the incident photon frequency $c_1 = 0.1$, the normal EP coupling $\lambda_1 = 0.14$ and the DJT coupling $\lambda_2 = 0.10$.

The Raman spectral intensity or the phonon SDF is plotted in figure 2 for a given temperature $t = 0.001$, where the superconductivity and lattice strain coexist in the system. In absence of normal EP coupling i.e., $\lambda_1 = 0$, the phonon self-energy ($\sum(\omega, q) = 0$) is zero. Hence there appears a peak p_0 centered at $\tilde{\omega} = \frac{\omega}{\omega_0} = 1$ corresponding to the bare phonon frequency ($p = \frac{\omega_0}{2t_0} = 1$) for the long wave length optical phonon ($q = 0$). For a finite normal EP coupling ($\lambda_1 = 0.14$) and DJT coupling ($\lambda_2 = 0.10$) at finite temperature $t = 0.001$ with given SC gap ($z = 0.00952$) and lattice strain ($e' = g_1 \times e \simeq 0.0136$), the position of the

bare phonon peak p_0 shifts to the higher frequencies i.e., $\tilde{\omega} \simeq 1.05$ indicating the hardening behavior of the phonon frequency due to renormalization effect. For these two given values of λ_1 and λ_2 there appears two new Raman active peaks p_1 and p_2 at lower frequencies. The low frequency peak p_1 appears at energy $\tilde{\omega} \simeq 0.125$. This corresponds to the excitation energy of the peak i.e., $c_1 = p\tilde{\omega} \simeq 0.08 \times 0.125 = 0.010$. This energy is slightly higher than the SC gap energy $\Delta \simeq 0.00952$ at $t = 0.001$ as determined from figure 1. The slightly higher value obtained in the spectral function in figure 2 is due to other interaction including the DJT effect. Thus the peak p_1 arises due to the SC excitation gap. The second peak p_2 appearing at the frequency $\tilde{\omega} \simeq 0.245$, corresponds to an excitation energy of the peak i.e., $c_1 = p\tilde{\omega} \simeq 0.08 \times 0.245 = 0.0196$. This energy is slightly higher than, but close to the gap associated with JT distortion at $t = 0.001$ which is given by $e' = g_1 \times e = 0.0136$. So the peak p_2 appearing in the SDF can be attributed to the phonon excitation arising due to lattice distortion as the system undergoes a structural phase transition. The interplay of these two order parameters SC gap (z) and JT energy (e') is investigated below from figure 3 to 9.

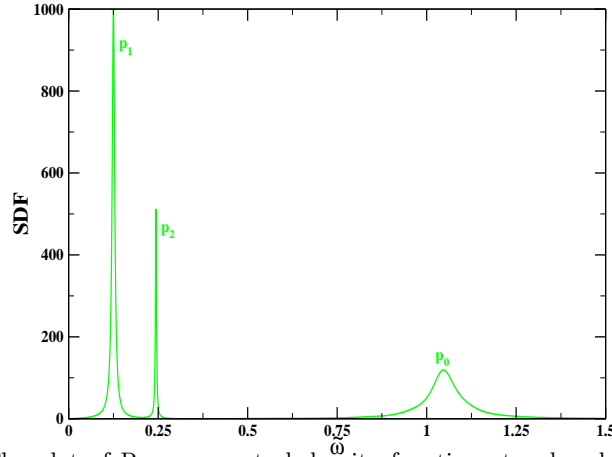


Fig. 2 The plot of Raman spectral density function at reduced temperature $t = 0.001$ ($z = 0.00952$, $e' = 0.0136$) for the above set of values and the suitable values of bare phono frequency $p = 0.08$ and spectral width $e_1 = 0.004$.

Figure 3 shows the plot of SDW vs $\tilde{\omega}$ for different values of temperature $t = 0 - 0.0023$ and for other fixed parameters. The self-consistent plot of z and e' shown in figure 1 indicates that the SC order and JT energy coexist upto the SC transition temperature $t_c \simeq 0.0052$. The temperature dependence of SDF displays the interplay of the SC and JT gaps as shown in figure 3. With the increase of temperature from $t = 0$ to 0.0023 in the coexistence phase the peak position of the SC gap move towards higher energies and the peak position of the JT gap excitation peak moves towards lower energies and merge each other at temperature $t = 0.0022$. On further increasing the temperature, the spectral height of the merged peak is

suppressed accompanied by a larger spectral width and finally vanish at $t > 0.0023$, which is smaller than the SC transition temperature. This SC peak in coexistence phase vanishes due to the interaction of static and dynamic JT effect displaying a strong interaction between them.

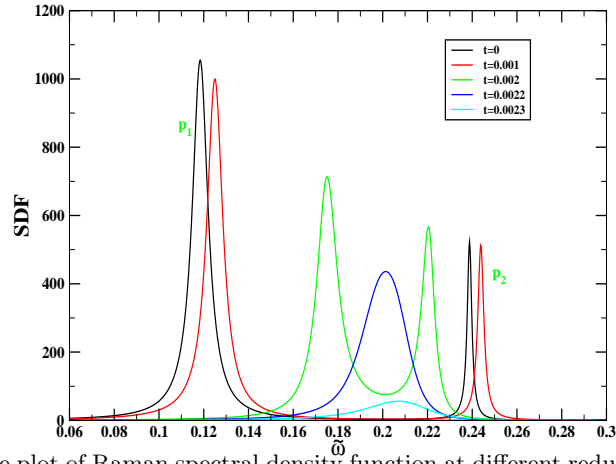


Fig. 3 The plot of Raman spectral density function at different reduced temperatures $t = 0.0, 0.001, 0.002, 0.0022$ and 0.0023 .

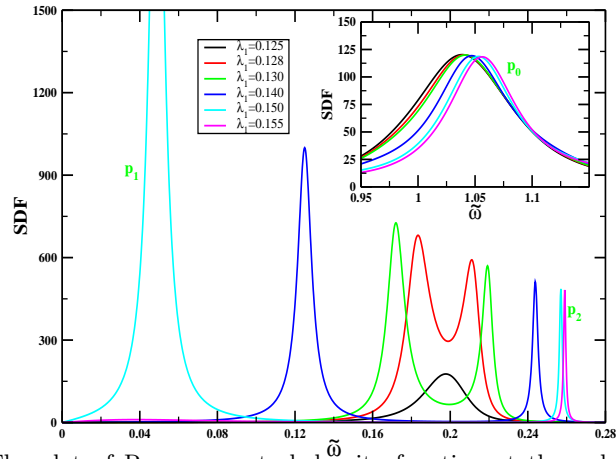


Fig. 4 The plot of Raman spectral density function at the reduced temperature $t = 0.001$ for different values of the normal EP coupling $\lambda_1 = 0.125, 0.128, 0.13, 0.0, 0.15$ and 0.155 .

Figure 4 shows the effect of normal EP coupling (λ_1) on the two Raman active peaks. At very low value of EP coupling ($\lambda_1 = 0.125$) the two excitation peaks merge with each other and appear as one peak at energy $\tilde{\omega} = 0.2$. As λ_1 increases,

the single peak splits into two separating the low energy SC excitation peak p_1 from the high energy JT distortion peak p_2 . With the further increase of λ_1 the JT peak p_2 moves to higher energies and the SC peak p_1 move to lower energies, finally for a higher value of normal EP coupling $\lambda_1 \simeq 0.155$, the SC peak p_1 nearly vanishes and the high energy JT peak exists. The inset of figure 4 shows the effect of the normal EP coupling on the bare phonon frequency peak p_0 . When the normal EP coupling λ_1 increases from 0.125 to 0.155, the spectral weight of bare phonon frequency p_0 shifts to higher energies exhibiting the hardening behaviour of the phonon mode.

Figure 5 shows the SDF vs $\tilde{\omega}$ for different values of DJT coupling (λ_2). In absence of DJT coupling ($\lambda_2 = 0$) two peaks p_1 and p_2 appear due to the normal EP coupling (λ_1). With increase of DJT coupling the JT excitation peak p_2 shifts towards the lower energies with slightly enhancement in spectral height. This decrease in JT energy of the peak p_2 with increase of DJT coupling is consistent with our earlier result obtained from the self-consistent solution of SC gap and JT energy gap¹⁸. On the other hand with increase of the DJT coupling (λ_2) the position of the SC excitation peak shifts to higher energies with a monotonically decrease in spectral height. This suggests that the DJT coupling suppresses the JT gap and consequently enhances the SC gap. The inset of figure 5 shows the effect of the DJT coupling on the bare phonon frequency peak p_0 . When the DJT coupling is increased from $\lambda_2 = 0.0$ to 0.25, the bare phonon frequency shows neither appreciable change in its spectral width nor its spectral height.

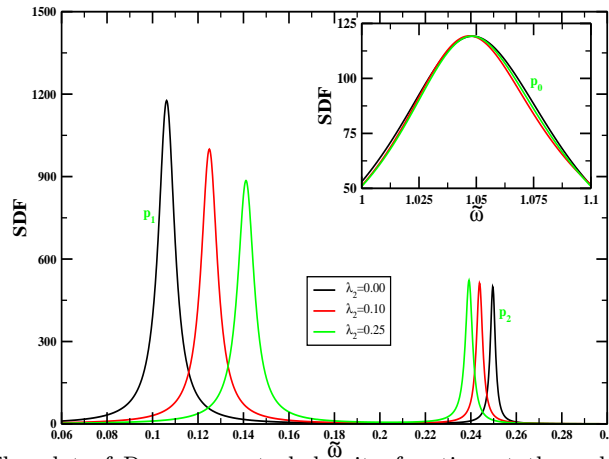


Fig. 5 The plot of Raman spectral density function at the reduced temperature $t = 0.001$ for different values of the dynamic EP coupling $\lambda_2 = 0.0, 0.10$ and 0.25 .

Figure 6 shows the plot SDF vs $\tilde{\omega}$ for different values of SC coupling from $g = 0.0280$ to 0.0350 . For a moderately high value of SC coupling $g = 0.0350$, the SC excitation peak p_1 and the JT gap excitation peak p_2 are well separated and the JT excitation peak p_2 shifts to lower energies with gradual increase of spectral height. This suggests that with decrease of SC coupling the JT gap is suppressed

and in consequence the SC gap is enhanced considerably. On further decreasing SC coupling, two excitation peaks appear to merge for $g = 0.0285$ and finally merged for $g = 0.0280$ with considerably suppression of the spectral height and with more decrease of the SC coupling the merged peak will vanish completely. The inset of figure 6 shows the effect of the SC coupling on the bare phonon frequency peak p_0 . When the SC coupling increases, the spectral weight shifts from lower to the higher energies exhibiting the hardening behaviour of the phonon mode and the spectral height shows no appreciable change.

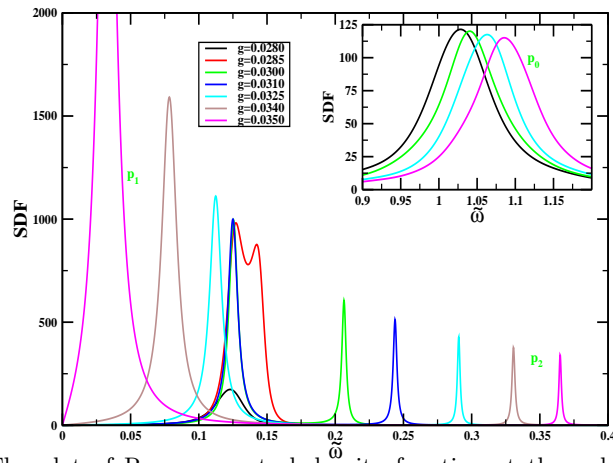


Fig. 6 The plot of Raman spectral density function at the reduced temperature $t = 0.001$ for different values of the SC coupling $g = 0.0280, 0.0285, 0.0300, 0.0310, 0.0325, 0.0340$ and 0.0350 .

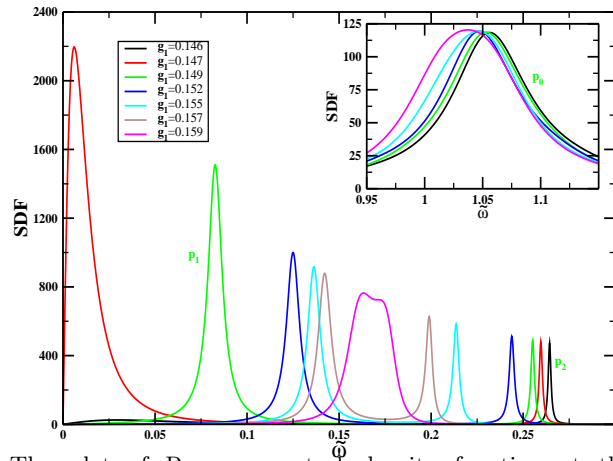


Fig. 7 The plot of Raman spectral density function at the reduced tem-

perature $t = 0.001$ for different values of the JT coupling constant $g_1 = 0.146, 0.147, 0.149, 0.152, 0.155, 0.157$ and 0.159 .

Figure 7 shows the effect of static JT coupling on Raman spectral peaks of the system. For a lower static JT coupling $g_1 = 0.146$, the JT excitation peak p_2 appears at higher energy $\tilde{\omega} \simeq 0.265$ but the SC excitation peak appears as a very flat peak at lower energy. With increase of JT coupling, the JT excitation peak p_2 shifts towards the lower energies indicating the suppression of JT gap while the SC excitation peak position shifts towards higher energies with a corresponding decrease in spectral height, indicating the enhancement of SC gap with g_1 . This is consistent with our conclusion from figure 1 that the suppression of JT energy induces the enhancement of magnitude of the SC gap. Finally for a static JT coupling $g_1 = 0.159$, two excitation peaks tend to merge to give rise a single peak, where the SC gap tends to be equal to the JT gap. With the further increase of the JT coupling the two peaks will merge with decrease in spectral height and will finally be suppressed completely. The inset of figure 7 shows the effect of the static JT coupling on the bare phonon frequency peak p_0 . It is observed that, with the increase of the static JT coupling g_1 , the spectral weight of the phonon frequency mode shifts to lower energies exhibiting its softening behaviour, but there is no appreciable change in spectral height but some increase in spectral width.

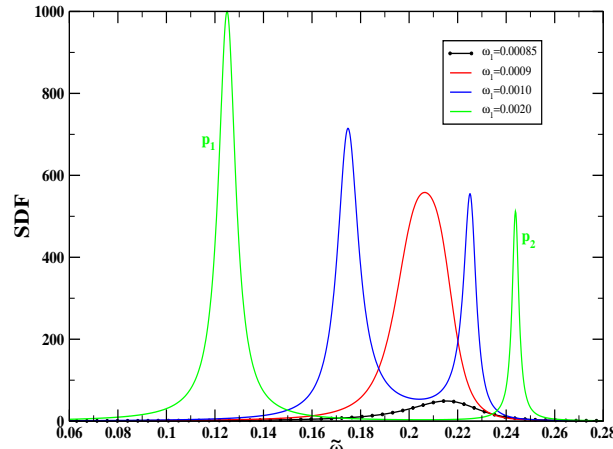


Fig. 8 The plot of Raman spectral density function at the reduced temperature $t = 0.001$ for different values of the phonon vibrational frequency $\omega_1 = 0.00085, 0.0009, 0.0010$ and 0.0020 .

Figure 8 shows the plot of SDF vs $\tilde{\omega}$ for different values of phonon vibrational frequency ω_1 at any finite temperature. It is observed from the figure that a single peak appears in the SDF for very low phonon vibrational frequency $\omega_1 = 0.00085$. The spectral height of the single peak is enhanced with increase of phonon vibrational frequency to $\omega_1 = 0.0009$. On further increase in ω_1 to 0.0010 and 0.0020 the single peak splits into two giving rise to high frequency JT excitation peak p_2

and SC gap excitation peak p_1 at low frequency. In other hand the increase of frequency ω_1 the magnitude of the JT gap is enhanced to higher energy, while the SC gap is suppressed to a lower energy. The separation between the two gaps gradually increases with the increase of ω_1 resulting in weak interplay between these two interactions.

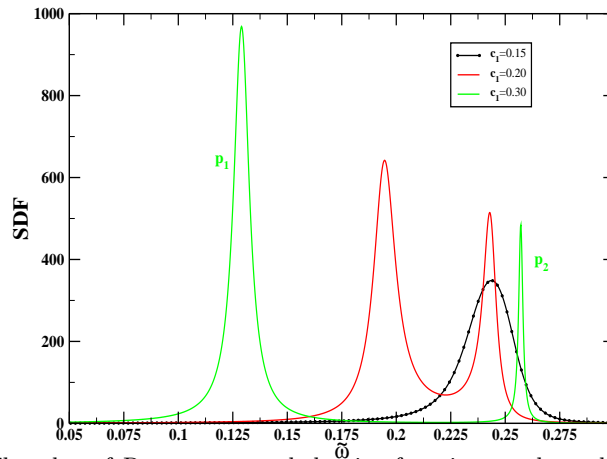


Fig. 9 The plot of Raman spectral density function at the reduced temperature $t = 0.001$ for different values of the reduced incident photon frequency $c_1 = 0.15, 0.20$ and 0.30 .

Figure 9 shows the plot of SDF vs $\tilde{\omega}$ for different values of incident photon frequency $c_1 = \frac{\omega}{2t_0}$. For lower incident photon frequency $c_1 = 0.15$ a single symmetric excitation peak appears at energy $\tilde{\omega} \simeq 0.24$ in the SDF. Here the SC gap energy and JT gap energy are equal. With increase of photon frequency c_1 to 0.20 and 0.30 the single peak splits into two giving rise to the low frequency SC gap excitation peak p_1 at lower energies and the high frequency JT gap excitation peak p_2 at higher energies. Thus this is consistent with our conclusion from figure 1 that the increase of JT distortion gap tends to suppress the SC gap and this shows a clear interplay of SC and JT order parameters.

7. Conclusion

The present calculation has been carried out for a system which exhibits the coexistence of s -wave type superconducting state and the static and dynamic Jahn-Teller distortion. The results of this calculation may be applied to some cuprate superconductors like the bismuthates⁸. The phonon SDF is calculated by the Green's function technique for the coexistence phase of the superconductivity and lattice strain in presence of DJT coupling. The SDF displays three peaks i.e., the peak p_0 centered at energy $\tilde{\omega} \simeq 1.05$ for the renormalized bare phonons, the peak p_1 at energy $\tilde{\omega} \simeq 0.125$ representing the SC gap excitation and the peak p_2 at energy

$\tilde{\omega} \simeq 0.245$ representing the gap excitation associated with the JT distortion. The interplay of these two long range orders are investigated by varying the normal EP coupling (λ_1), the static JT coupling (g_1), the DJT coupling (λ_2), the SC coupling (g), temperature (t), phonon vibrational frequency (ω_1) and incident photon frequency (c_1). It is observed that the normal EP coupling (λ_1) enhances the JT gap and suppresses the SC gap. As a result JT excitation peak shifts to the higher energies while SC gap excitation peak shifts to the lower energies. It is observed that both the static and dynamic Jahn-Teller couplings g_1 and λ_2 suppress the insulating JT gap and enhance the SC gap and as a result with increase of g_1 and λ_2 the JT excitation peak shifts to the lower energies and the position of the SC excitation peak shifts to the higher energies. From the study of the effects of phonon vibrational frequency (ω_1) and the incident photon frequency (c_1) it is observed that both the frequencies ω_1 and c_1 induce higher JT distortion leading to suppression of the SC gap. Under this condition of increasing ω_1 and c_1 the SC excitation peak p_1 and JT excitation peak p_2 are gradually separated from each other. The present study displays a very strong interplay between SC interaction, static JT interaction as well as DJT interaction.

Acknowledgements

The authors gracefully acknowledge the research facilities offered by the Institute of Physics, Bhubaneswar, India during their short stay.

References

1. D. McK. Paul, G. Balakrishnan, N.R. Bernhoeff, W.I.F. Davia and W.T.A. Harrison, *Phys. Rev. Lett.* **58** (1987) 1976.
2. P. Day, M. Rosseinsky, K. Prassides, W.I.F. David, O. Moze and A. Soper, *J. Phys. C* **20** (1987) 1429.
3. M. Lang, R. Kürsh, A. Grauel, C. Geibel, F. Steglich, H. Rietschel, T. Wolf, Y. Hidaka, K. Kumagai, Y. Maeno and T. Fugita, *Phys. Rev. Lett.* **69** (1992) 482.
4. D.T. Keane, G.A. Held, J.L. Jordan-Sweet, M.W. Shafer, P.M. Horn, G. Guntherodt, J. Langen, M. Weit, A. Erle, S. Blumenroder and E. Zirngiebl, *Physica C* **153-155** (1988) 594.
5. J.D. Axe, A.H. Moudden, D. Hohlwein, D.E. Cox, K.M. Mohanty, A.R. Moodenbaugh and Youwen Xu, *Phys. Rev. Lett.* **62** (1989) 2751.
6. H. Takagi, R.J. Cava, M. Marezio, B. Batlogg, J.J. Krajewski, W.F. Peck. Jr., P. Border and D.E. Cox, *Phys. Rev. Lett.* **68** (1992) 3777.
7. M. Sato, in *Physics of High Temperature Superconductivity* (Springer, Berlin, 1992) p.237.
8. S. Sugai, S. Uchida, K. Kitazawa, S. Tanaka and A. Katsui, *Phys. Rev. Lett.* **55** (1985) 426.
9. M.K. Crawford, M.N. Kunchur, W.E. Farneth, E.M. McCarron III and S.J. Poon, *Phys. Rev. B* **4** (1990) 282.
10. M.K. Crawford, W.E. Farneth, E.M. McCarron III, R.L. Harlow and A.H. Moudden, *Science* **250** (1990) 1390.
11. R. Sooryakumar, M.V. Klein, *Phys. Rev. Lett.* **45** (1980) 660.

18 *B. K. Raj, B. Pradhan and G. C. Rout*

12. R. Sooryakumar, M.V. Klein, *Phys. Rev. B* **23** (1981) 3213.
13. C.A. Balseiro, L.M. Falicov, *Phys. Rev. Lett.* **45** (1980) 662.
14. P.B. Littlewood, C.M. Varma, *Phys. Rev. Lett.* **47** (1981) 811.
15. G.C. Mohanty, S.N. Behera, *Cand. J. Phys.* **61** (1983) 1160.
16. S.N. Behera, S.G. Mishra, *Phys. Rev. B* **31** (1985) 2773.
17. G.C. Rout, B. Pradhan, S.N. Behera, *Physica C* **444** (2006) 23.
18. B.K. Raj, B. Pradhan and G.C. Rout, arXiv:1210.7743 (2012).
19. G.C. Rout, B. Pradhan, S.N. Behera, *phys. stat. solidi (c)* **3** (2006) 3617.
20. B. Pradhan, K.L. Mohanta, G.C. Rout, *Physica C* **475** (2012) 14.
21. K.A. Müller, *Philos. Mag. Letter* **82**, 270 (2002).
22. K.A. Müller, *J. Supercond. Nov. Mag.* **17**, 3 (2004).
23. Guo-Meng Zhao, *Philos. Mag. Letter* **84**, 3861 (2004).
24. D.N. Zubarev, *Sov. Phys. Usp.* **3** (1960) 320.